Elucidation of Enhanced Lithium Conductivity in Nanoporous Ionogel Using Solid State NMR

Weijers, Mark; Karanth, Pranav; Ganapathy, Swapna; Mulder, Fokko M.

DOI
10.1002/admi.202201646

Publication date
2022

Document Version
Final published version

Published in
Advanced Materials Interfaces

ADVANCED MATERIALS INTERFACES
www.advmatinterfaces.de

Elucidation of Enhanced Lithium Conductivity in Nanoporous Ionogel Using Solid State NMR

Mark Weijers, Pranav Karanth, Swapna Ganapathy, and Fokko M. Mulder**

Nanostructured solid composite electrolyte or nano-SCE, which is composed of an ionic liquid, nanoporous silica, and residuals of immobilized precursor components, shows promising synergistic properties. The ionic conductivity of nano-SCE is in the range of 2–5 mS cm^{-1}, which exceeds the bulk ionic liquid conductivity at ambient temperature, while maintaining characteristics of a solid electrolyte such as having no leakage issues as the ionic liquid is confined, and lower flammability compared to conventional liquid electrolytes. In this study, the underlying mechanism of enhanced conductivity is investigated by using magic angle spinning NMR and NMR relaxometry analysis. Water, one of the volatile precursor molecules has shown to play a key role in the final conductivity and stability at the solid-electrolyte interface, as it enhances the temperature range in which the ionic liquid remains mobile. In line with previous studies, water with lowered mobility is found in the silicon matrix. The activation energies of lithium ion transfer probed by NMR relaxometry, however, do not change as function of water content. The increase in bulk mobility of lithium ions under ambient conditions compared to water-less nano-SCE is found to be the origin of the altered conductivity of this material.

1. Introduction

Solid composite electrolytes consisting of a porous polymer or silicon solid matrix, combined with an ionic liquid electrolyte (ILE) show promising characteristics in EV battery applications. By combining a morphology structuring compound with an ionic liquid, conductivities nearing conventional liquid electrolytes are achieved while nonflammability,[1] bendability, and strength characteristics of a solid electrolyte are maintained.[2]

Hybrid electrolytes may have synergistic properties enhancing mechanical strength, ionic conductivity and/or mechanical, or thermal stability.[3,4] The of sol–gel processed ionogels form composites in situ, which is a different approach than physical mixture composites in example.[3–7] Recently Sagara et al. found synergistic properties of the lithium-bis((fluorosulfonyl) imide/1-ethyl-3-methylimidazolium bis(fluorosulfonyl)imide (Li-FSI/EMI-FSI) and lithium-bis((trifluoromethylsulfonyl) imide 1-butyl-1-methylpyrrolidinium bis(trifluoromethylsulfonyl)imide (Li-TFSI/BMP-TFSI) ILEs combined with a silicon network in which the obtained gel showed better lithium ion conductivities than the bulk ionic liquid.[8,9] In this work the ionogel shows similar rate performance compared to conventional liquid electrolyte $LiPF_6$ in EC:DMC in Li-LFP battery cells. Chen et al.[10] proposed that the origin of this behavior that is, increase in lithium conductivity in nano-SCE is facilitated by the de-solvation of the lithium ions. In this work lithium-bis((trifluoromethyl)sulfonyl)imide/1-ethyl-3-methylimidazolium bis(trifluoromethylsulfonyl)imide (Li-TFSI/EMI-TFSI) ILE is used (**Figure 1**). Previously it has been shown that porous silica networks show several mechanisms which lead to a change in the diffusivity of the various mobile species. Guyomard-Lack et al. show that lithium diffusivity is an interplay between surface and bulk associated lithium concentrations.[11] The two environments are further elucidated by Jayakody et al. who show two diffusion regimes by varying pore sizes, restrictive diffusion at the surface and long ranged diffusion in the bulk.[12] For nano-SCE comprising of SiO_2, ILE and water, the silanol hydroxyl bonds are thought to be (partially) covered by water molecules.[10] In this structure, the TFSI anion hydrogen bonds through their O=S=O group with these immobilized water molecules. The EMI cations would show increased affinity compared to lithium cations with the formed TFSI layer through hydrogen bonding. As a result, with the proper number of water molecules, an immobile "glacial" layer is formed on the silicon backbone and charge layers emerge of which the layer next to water molecules consists predominantly of hydrogen bond making EMI cations. The charge layers form a dipole of which the TFSI associated to lithium is drawn, which leads to a lower net activation energy of lithium mobility. As this type of diffusion

M. Weijers, P. Karanth, F. M. Mulder
Faculty of Applied Sciences
Chemical Engineering Department
Delft University of Technology
Van der Maasweg 9, Delft 2629HZ, The Netherlands
E-mail: weijers.mj@gmail.com; F.M.Mulder@tudelft.nl
S. Ganapathy
Department of Radiation Science and Technology
Delft University of Technology
Mekelweg 15, Delft 2629JB, The Netherlands
The ORCID identification number(s) for the author(s) of this article can be found under https://doi.org/10.1002/admi.202201646.

DOI: 10.1002/admi.202201646

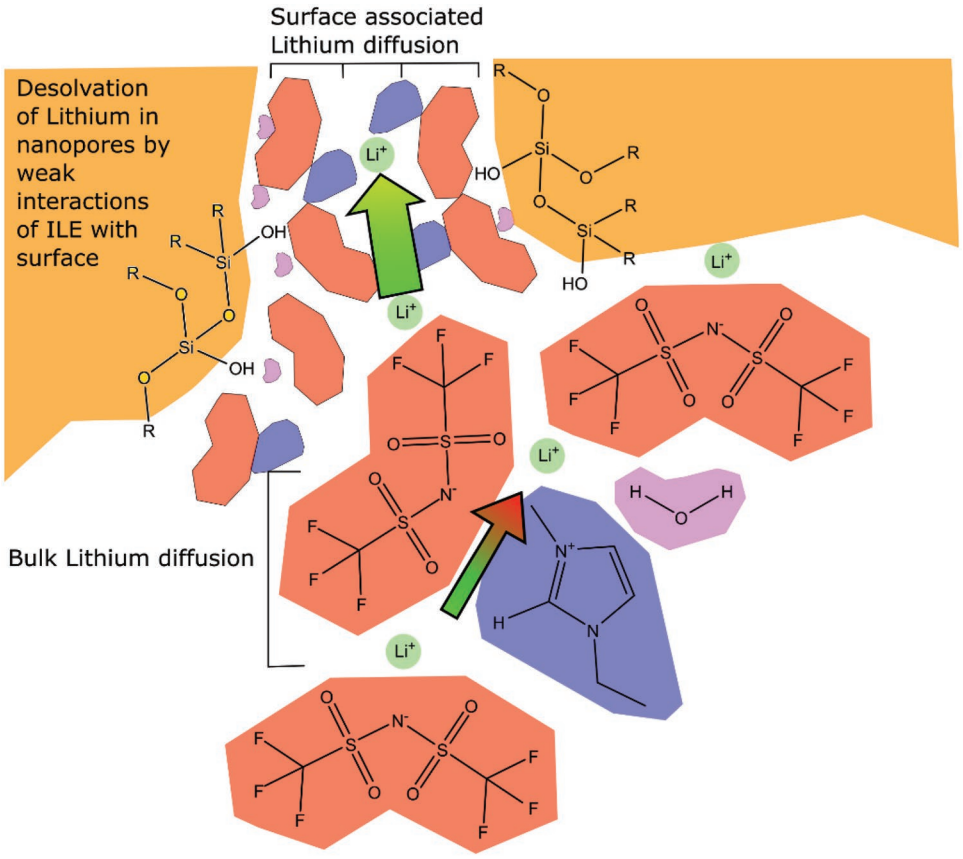

Figure 1. Interplay with silicon backbone surface and ILE. TFSI and EMI are thought to have preferred orientations toward the surface, facilitated with water. This causes the lithium metal to desolvate and become highly mobile.

is dependent on the presence of a polymer backbone, this is called surface associated diffusion.

In ILE polymer hybrid systems, both surface associated and bulk lithium diffusion can be expected as pore geometry and sizes vary in the network. Jayakody et al. describe a method to investigate surface and bulk associated lithium.[12] A necessary characteristic for the surface lithium is that its residence lifetime is longer than the translational correlation time in the bulk to enable distinguishing the two environments. Net conductivity can be expected to drop in polymer systems as steric effects of the polymer network create more tortuous diffusion pathways of the mobile species compared to bulk liquids. Surface associated diffusivity can however play a role in altering the mobility of specific molecular species, specifically Li^+.

In this study, NMR techniques are used to elucidate the structure/ion mobility relation of the nano-SCE components. The conductivity of lithium ions measured by electrochemical impedance spectroscopy (EIS) is compared to that obtained with static relaxometry using nano-SCE samples containing varying amounts of water. In this way the dependence of the concentration of the volatile components to the local and bulk energetics of various diffusional processes could be elucidated. A comprehensive method and complete derivation of the self-diffusion constant from relaxometry data is described in detail by Uitz et al.[13] and McDowell et al.[14] respectively, using a model introduced by Bloembergen, Purcell, and Pound.[15] Considerations and equations for relaxometry fitting are included in Supporting Information.

2. Results

Nano-SCE is prepared by a one pot synthesis of liquid precursors. This may allow its penetration in porous materials like battery electrodes before polymerization.[8] During synthesis, a typical solvent supported, slightly alkaline, sol–gel formation process is taking place. Of the various possible polymerization rate coefficients for tetra-ethyl-orthosilicate polymerization intermediates, $Si(OCH_3CH_2OH)_X(OH)_Y(OSi)_Z$, to polymerize only three rates are determining in acid supported polymerization.[16] In slightly alkaline solutions however, after hydrolysis, the deprotonated silanol group is able to attack more acidic silanol groups which leads to increased branching compared to the acidic polymerization process.[17,18] The result is a flexible finely branched colloidal structured gel which can be dried to a more condensed sol–gel by removing the solvent 1-methoxy-2-propanol (PGME) and water using conventional drying.[19]

The acidity of the solution in this initial process is very sensitive. Modification of alkaline conditions by addition of lithium hydroxide to pH 11 did not result in successful gel formation, showing the delicate conditions in which polymerization takes place. In the confined structure, the majority of unbranched

silane sites which are unavailable for condensation are hydrolyzed if the polymerization product is sufficiently diluted during the polymerization step.

After gel formation the volatile precursors are removed slowly to maintain structural integrity of the material. This process is monitored by weighing the sample after each drying step as shown in Figure S20, Supporting Information for reference. After the initial polymerization process the extent of drying is 17%. Subsequent 800 and 200 mBarA drying steps yield 49% and 69% extent of drying. Further high vacuum treatments (HVT) at 0.3 mBarA and 60 °C yields 98%–100% extent of drying overnight, that is, essentially complete removal of ethanol, water, and PGME. Samples called nano-SCE were prepared without the HVT treatment. After 3.5 h HVT a sample was taken called Semi-dry nano-SCE (Table S2, Supporting Information for an overview).

The obtained nano-SCE gel has interesting mechanical characteristics. The sample is slightly bendable but it easily fractures upon puncturing with for example, a spatula. Upon fracturing, typically complete breakage of the material that is parallel with the spatula edge is observed. The parts do easily adhere together, but the material does not cure upon re-contacting. This indicates that the polymerization process has finished and only weak molecular interactions cause grain/grain adhesion, together with ionic liquid surface tension. The material is leakage free in normal circumstances. Centrifugation at 6000 rcf does not show phase separation of ionic liquid from the nano-SCE and the material shows stable performance after 1 year of storage in a glove box. The ionic liquid can however separate out of the nano-SCE after compressing as a sponge-like feature, which leads to formation of droplets observed after removing the compressed particles. After washing the gel with acetone extensively and subsequent drying in a vacuum oven, sand-like particles are obtained which show smooth fracturing planes as can be seen in the SEM image given in **Figure 2**A. Its surface structure shown in Figure 2B is rough, indicating that fracturing does not expose a clean facet.

A verification of the electrochemical characteristics is provided to ensure a similar material is made compared to other nano-SCE's reported previously.[8] Conductivities of the three SCE were measured using EIS in symmetric Li |SCE | Li cells. The resistance at the touchdown point at high frequencies of the Nyquist plot are taken as the electrolyte resistance at room temperature.[20] Conductivities are subsequently calculated using the pellet geometry detailed in Experimental Section. After EIS, samples were subjected to potentiostatic polarization of 80 mV for 1 h and the EIS spectrum was re-measured. Obtained values before and after a few repeats of the polarization process are shown in **Figure 3**A (Some Nyquist plots are shown in Figures S8–S10, Supporting Information).

Nano-SCE shows a high conductivity compared to the bulk ionic liquid, which is in line with the findings of Sagara et al.[10] However after potentiostatic polarization both a decrease in conductivity and a large increase in charge transfer resistance is measured, indicating the change of the bulk conductivity is in concert with solid–electrolyte interface (SEI) formation on the lithium surface (Figure S8, Supporting Information). Nano-SCE was repeatedly subjected to galvanostatic polarization and the bulk conductivity subsequently measured kept decreasing, indicating that the presence of the initial volatile components in nano-SCE cause continuing side reactions.

The contribution of the volatile solvents to the stability was further tested by drying nano-SCE at 60 °C at 0.3 mBarA vacuum for an extended period removing the volatile components, yielding dry-nano-SCE. Dry-nano-SCE shows a reduced conductivity compared to the nano-SCE but unlike nano-SCE maintains the same conductivity before and after polarization testing. Remarkably, for dry-nano-SCE, the contact resistance decreased after 12 h of extended polarization (Figure S9, Supporting Information). The conductivity of dry nano-SCE is in line with the conductivities found by Sagara et al.[8] and remains relatively high compared to other polymer electrolytes which have conductivity ranges of 10^{-2}–10^{0} mS cm^{-1}.[21]

The material stability is further tested with a galvanostatic cycling test. Symmetric Li-Li cells with ionic liquid EMI-TFSI and nano-SCE varieties are subjected to galvanostatic cycling for 70 days at 0.1 mA cm^{-2} (Figure 3B). Nano-SCE immediately shows high overpotentials indicating a high interfacial resistance. Semi-dry nano-SCE did not show stable cycling behavior (SI, Figure S7, Supporting Information). In case of dry nano-SCE, the overpotential decreases from 80 to 60 mV over the first 20 days, indicating an improved charge transfer, probably originating from improved contact between the lithium metal and dry nano-SCE interface. The dry-nano-SCE shows stable potential profiles for the complete duration of cycling.

Electrochemically the dry-nano-SCE behaves like an electrolyte with limited charge carrier density. Upon increasing the current to 1 mA cm^{-2}, the voltage profile shows continuous

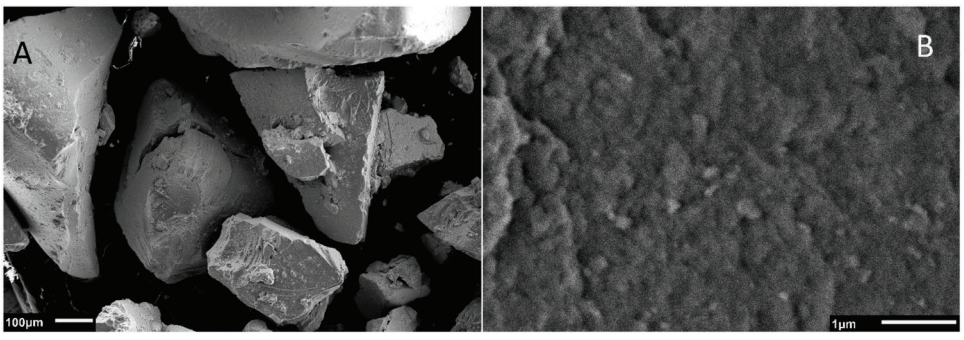

Figure 2. A,B) SEM images of acetone-washed nano-SCE. After material fracturing, quite smooth surfaces are observed with small debris attached on the surfaces (left). A higher magnification shows roughness in the sub-micron scale (right).

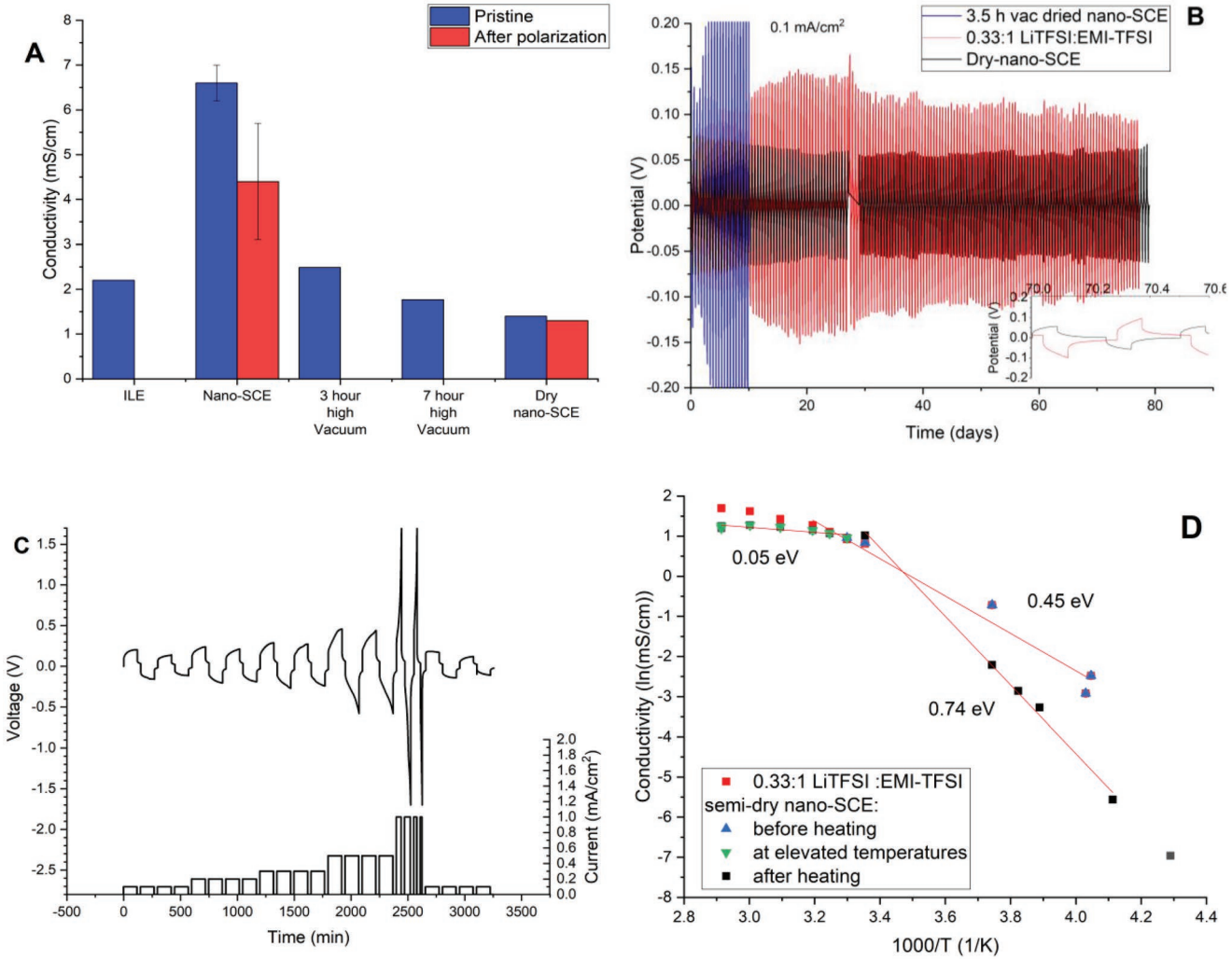

Figure 3. A) EIS derived conductivities of 0.33:1 LiTFSI:EMI-TFSI ILE and nano-SCE materials before and after polarization studies. The nano-SCE conductivity drops upon extended duration of drying. The error bars indicate different results by varying the potential window and duration of the polarization testing. B) Voltage profile during galvanostatic cycling at 0.1 mA cm^{-2} in Li|Electrolyte|Li cells of: 3.5 h vacuum dried nano-SCE (blue), dry-nano-SCE (black) and four glass fiber separators immersed with EMI-TFSI-based ILE (red). C) Voltage profile of dry-nano-SCE in Li|dry-nano-SCE|Li at galvanostatic cycling for 2 h with varying current densities. The cut-off potential of 1.7V is reached at a current of 1 mA cm^{-2}. D) EIS derived conductivity of semi-dry nano-SCE and ILE as function of temperature. Red lines indicate estimated linear regions of semi-dry nano-SCE. Before heating to 70 °C (blue, green) and after heating to 70 °C (black) show different characteristic slopes. At high temperatures bulk ILE 0.33:1 LiTFS:EMI-TFSI (red) is slightly higher compared to semi-dry nano-SCE (green).

polarization increase as seen from Figure 3C. Initially the potential seems to reach a plateau similar to lower currents, but then the potential starts to increase rapidly over time indicating concentration depletion. Such polarization buildup requires lithium and counter ions to move and therefore one may view it as bulk liquid diffusion that is the dominant mode of diffusion for dry-nano-SCE.

The role of volatiles in the bulk conductance becomes apparent from temperature dependent EIS measurements. The bulk activation energy of lithium conductivity is determined using the temperature dependent impedance of the high frequency region in a symmetric cell. Semi-dry-nano-SCE was tested for this, as it contains some volatiles and shows enhanced conductivity of the material compared to dry-nano-SCE. First the sample is cooled down to –40 °C, then it is heated up to 70 °C and finally the sample is cooled to ambient temperatures. A glass fiber immersed with 0.33:1 mol:mol Li-TFSI:EMI-TFSI (ILE) is also tested in the same setup to compare activation energies. The static resistance value originating from the intercept in the Nyquist plot are converted to conductivities using Ohm's law and plotted in Figure 3D. A shallow slope is observed for the semi-dry nano-SCE above 30 °C corresponding to an activation energy of 51.5 meV (green, Figure 3D). Both the conductivity and temperature dependence are slightly lower than the ILE in this temperature region (red, Figure 3D, 179.5 meV). A change of slope can be observed in the temperature range between –26 and +30 °C. In here a semi-linear regime is observed which gives an estimated activation energy of 0.45 eV (blue, Figure 3D). At –40 °C a conductivity value is found which does not follow this trend (gray, Figure 3D). After

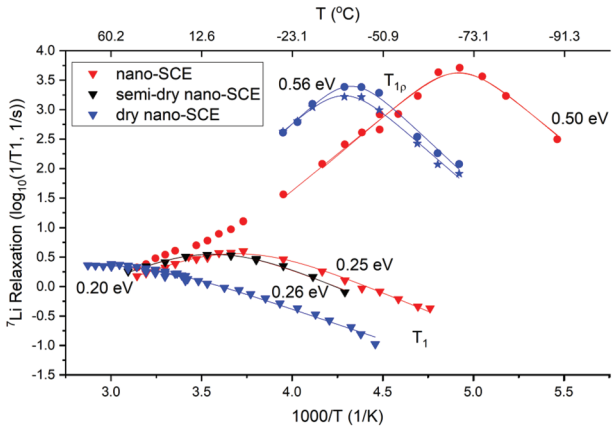

Figure 4. ^{7}Li relaxation in nano-SCE using various probing frequencies. Lines show fit region around the peak relaxation rate. Fits of $T_{1\rho}$ 12.5 kHz (circles), $T_{1\rho}$ 30 kHz (stars), and T_1 194.5 MHz (triangles) are fitted simultaneously.

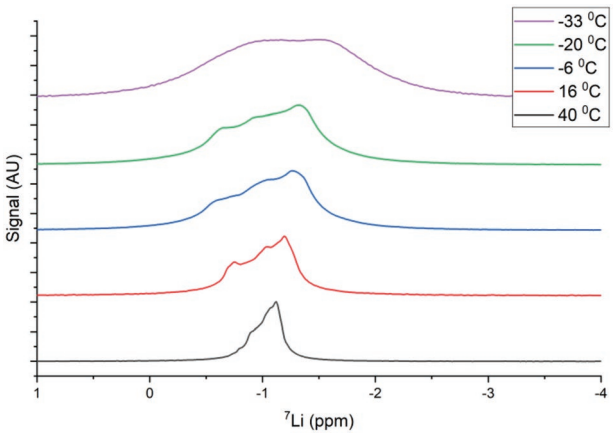

Figure 5. ^{7}Li static NMR spectra of nano-SCE as function of temperature.

heating to 70 °C however conductivities change in the low temperature region. A steeper slope corresponding to lower conductivities a higher activation energy of 0.74 eV is observed. This indicates that the volatile components are mobilized during heating to higher temperatures which allows them to migrate and react at the lithium interface during the experiment. The trend of the linear regime after heating extrapolates well to the –40 °C conductivity measured before heating, indicating that at this temperature, the volatiles did not play a significant role in the bulk conductivity in the first place. The presence of volatiles thus effectively lowers the bulk activation energy. This phenomenon is further explored with NMR to determine whether the lithium ion transfer mechanism itself changes, or if only the bulk mobility of all species are the cause of the overall lower activation energy.

Mobility of lithium ions and local activation energy barrier changes of lithium environments can be effectively probed by using NMR relaxometry techniques.[22] The ^{7}Li T_1 (ω_0 = 194.5 MHz) and $T_{1\rho}$ (ω_1 = 12.5 kHz) relaxation times are probed for the nano-SCE variants prepared with deuterated water between –90 and +100 °C. In **Figure 4**, the relaxation rates measured at various temperatures for nano-SCE, semi-dry nano-SCE and dry nano-SCE are shown. For all samples a maximum relaxation rate can be observed in the data, but at different temperatures.

Upon drying toward dry nano-SCE an upward shift in temperature can be observed for the highest relaxation rate ($1/T_1$) at which the correlation time (time between jumps) is of the order of the larmor frequency that is, $\tau_C \approx 1/\omega_0$. This indicates that the lithium ion mobility is reduced by the absence of the mobile volatile liquid species and the correlation time peak is only obtained when the solid dry-nano-SCE is heated to 60 °C.

The shape of the nano-SCE $T_{1\rho}$ and T_1 relaxation rate/temperature curves around the peak maxima are symmetric. Also the dry nano-SCE $T_{1\rho}$ curve is symmetric. Such a symmetric peak in the Arrhenius plot implies dominant uncorrelated self-diffusive type motion as given in the framework of the BPP (Bloembergen–Purcell–Pound) model.

For nano-SCE (red circles) the $1/T_{1\rho}$ shows a change in slope above 0 °C. The static ^{7}Li NMR spectrum around this temperature (**Figure 5**) shows a shift in dominant chemical environment, indicating the material surrounding the lithium changes around this temperature which is in line with the temperature dependent conductivities measured.

The redistribution of lithium over chemical environments or states will be the main reason for the change in relaxation rate for nano-SCE. The static ^{7}Li spectrum is resolved by fitting three peaks at temperatures above –20 °C and fitting two peaks below –20 °C (Figures S14 and S15, Supporting Information). The three peaks at –0.74, –1.07, and –1.22 ppm at 16 °C are assigned to three environments according to their characteristics: pore confined/ surface associated (broad, chemically shielded), intermediate IL layering (relatively broad, less chemically shielded) and bulk mobile lithium (sharp, least chemically shielded) in line with the interpretation of Guyomard-Lack et al. on lithium in an ionic liquid filled silica host.[23] The pore geometries present in the nano-SCE give a broad distribution of states for the confined lithium ions. For nano-SCE below –6 °C the relatively sharp peak around –1.22 ppm broadens and the signal fraction attributed to this environment lowers significantly (Figure 5). The same temperature can be identified as the region at which the slope of the $T_{1\rho}$ relaxation time starts to diverge in Figure 4. The change in slope can therefore be attributed to the change in dominant lithium environment from mobile to surface associated state upon cooling.

As the probing frequency of T_1 is high, T_1 relaxation probes fast processes (Larmor precession frequency, 194.5 MHz, ≈4 nanosecond range) while $T_{1\rho}$ probes relatively slow, long range processes (spin-lock frequency of 10–30 kHz, tens of microsecond range). The interpretation of the motions in terms of activated Li ion hopping or ionic liquid reorientations can be addressed by determining activation barriers from the Arrhenius behavior in Figure 4, but solely in the region in which the material does not show changes in dominant environment.

The activation energies of lithium transfer in the low frequency/low temperature regime only shows minor changes upon drying. The relaxation rate function is fit around the peak maxima using BPP derived equations assuming one activation energy (Section S1, Supporting Information).[14] These energies

associated with each environments motion are summarized in Table S1, Supporting Information. For the dry-nano-SCE, only a slightly higher activation energy is found compared to the nano-SCE indicating the apparent activation energy is locally fairly similar. Interestingly an opposite change in activation energy is observed for the fast lithium ion transfer process probed by T_1 relaxation at higher temperatures. The activation energy decreases from 0.25 to 0.21 eV after drying. The rationale for such lower barrier for diffusion of Li may be the increased ion concentration which lowers the hopping distance. At these higher temperatures desolvation of lithium through preferred hydrogen bonding of the TFSI molecule with surface layers are expected to only play a small role. The changes in E_A are remarkably enough relatively small considering the small plasticizing solvent molecules are fully removed.

The temperatures at which the maximum relaxation rates occur shows a pronounced shift when volatiles are removed. Mobility of ions influenced by viscosity and mixing effects is thus thought to be the major contributor to apparent barriers in the lithium ion diffusion process. The temperature regions at which the presence of volatile solvent shows increased conductivity of the bulk material is in line with the temperature regions at which the activation energies of a long range lithium hops are lower.

An estimate of the conductivity by using the activation energy and characteristic hop time obtained from Figure 4 curve fitting might elucidate which of the two environments play a dominant role in the bulk conductivity. Using Arrhenius Equation (S4), Supporting Information a hopping time τ at a certain temperature is calculated. The self-diffusion coefficient may then be estimated from concentration derived distance r by using Equation (1).

$$D = \frac{r^2}{6\tau} \tag{1}$$

The characteristic hop time is derived from the fit at the maximum relaxation rate condition, yielding diffusion coefficients in the order of 10^{-11} to 10^{-10} m^2 s^{-1} This is of the same order as that obtained for the high temperature region of the ionogel system investigated by Jayakody.[12] The dry-nano-SCE shows this diffusivity around 50–70 °C, where similar diffusivities were also found by Jayakody et al. Strikingly, nano-SCE has the same order of diffusivity already at 4 °C, at which temperature typical ionogels normally show diffusivities around 10^{-12} m^2 s^{-1}. Using the Nernst–Einstein relationship (Equation (2)),[24] an estimate of the conductivity is derived. Here AC conductivity σ_{AC} is derived as function of the lithium concentration c_{li+}, diffusion constant D, Faraday constant F, molar gas constant R, and the temperature T.

$$\sigma_{AC} = \frac{c_{Li^+} D F^2}{RT} \tag{2}$$

With the diffusion coefficient estimates of T_1 and $T_{1\rho}$ of dry nano-SCE, room temperature conductivities of 1.12 and 0.08 mS cm^{-1} were calculated respectively. The calculated conductivity from T_1 measurements is in fair agreement with the EIS study, indicating the mobile lithium/high temperature characteristics are the main contributor to the net conductivity. Similarly for the nano-SCE the conductivity derived from T_1 and $T_{1\rho}$ gives 6.78 and 1.29 mS cm^{-1} respectively. It thus appears the fast transfer process probed by T_1 shows the temperature region and chemical environment resulting in conductive motion. The change in the dominant lithium environment upon cooling shows the shift of lithium from this conductive environment thus best explaining the higher apparent activation energy measured by temperature dependent EIS.

So far the chemical composition changes of nano-SCE with varying amounts of water has to our knowledge not been studied, while understanding the presence and mobility of the volatile molecules is key for the increased conduction mechanism. The molecular species present in the material are probed by magic angle spinning (MAS) NMR. The materials synthesis involves the following reaction steps: ethyl groups of the TEOS molecule are hydrolyzed by available (deuterated) water. The hydroxyl group of the silicate subsequently condenses with other partially hydrolyzed silicate groups leaving water, ethanol the solvent PGME and ionic liquid in the solution.[18] The resulting structure contains the ionic liquid, a polymerized silica network and water. PGME and ethanol remain from the synthesis and their amounts depend on the drying stage of the nano-SCE. These components can all be visualized by NMR spectroscopy.

The ^{1}H NMR spectrum of nano-SCE (**Figure 6**A, red) does not show an apparent narrow liquid water signature around 4–5 ppm, which is consistent with the notion of frozen surface layer of water in the structure as probed using IR spectroscopy proposed by Chen et al.[10] To elucidate if water is present in the solid form, deuterated water is used to prepare the nano-SCE. The proton spectrum of this deuterated sample is compared to the original protonated sample as shown in black in Figure 6A. Peaks corresponding to EMI (≈1.41, 3.81, 4.1, 7.31, 7.38, and 8.45 ppm)[25] and PGME (≈1.15, 3.35 ppm) were resolved. In the deuterated sample no signature of water is resolved in the ^{1}H NMR spectrum and also a slight decrease in peak intensity at 8.47 ppm is observed. The ^{2}D MAS-NMR spectrum of the deuterated nano-SCE does show two broad peaks at 3.81 and 8.36 ppm (Figure 6B, red) indicating ^{2}D from the water has transferred partially to the central proton position on the imidazolium ring of the EMI molecule.

This prompted to probe the active exchange of the two deuterium environments. The peak at 8.36 ppm is associated with the highly polar single proton between the nitrogen groups in the imidazolium ring of the EMI molecule. The relative peak intensity of the proton peak at 8.36 ppm compared to other protons in the proton spectrum is lowered in the nano-SCE (Figure 6A, inset) indicating a fraction of the protons has exchanged with deuterium. With nuclear Overhauser effect spectroscopy (NOESY, Figure 6D) is shown that the two environments are not having cross-peaks, indicating no active exchange in the material on the timescale of the exchange period. A control test was performed by mixing D_2O with ILE and on probing the ^{2}D environments, a peak around 8.36 was not observed. This indicates that the exchange process is not spontaneous but catalyzed by the environment during sol–gel formation. The central proton on the imidazolium ring is known to have strong affinity with the anions[26] and is reported to be a reactive site in acid–base reactions.[27,28]

Comparison of signal broadening of the two deuterium environments (Figure 6C) shows that volatiles become immobile

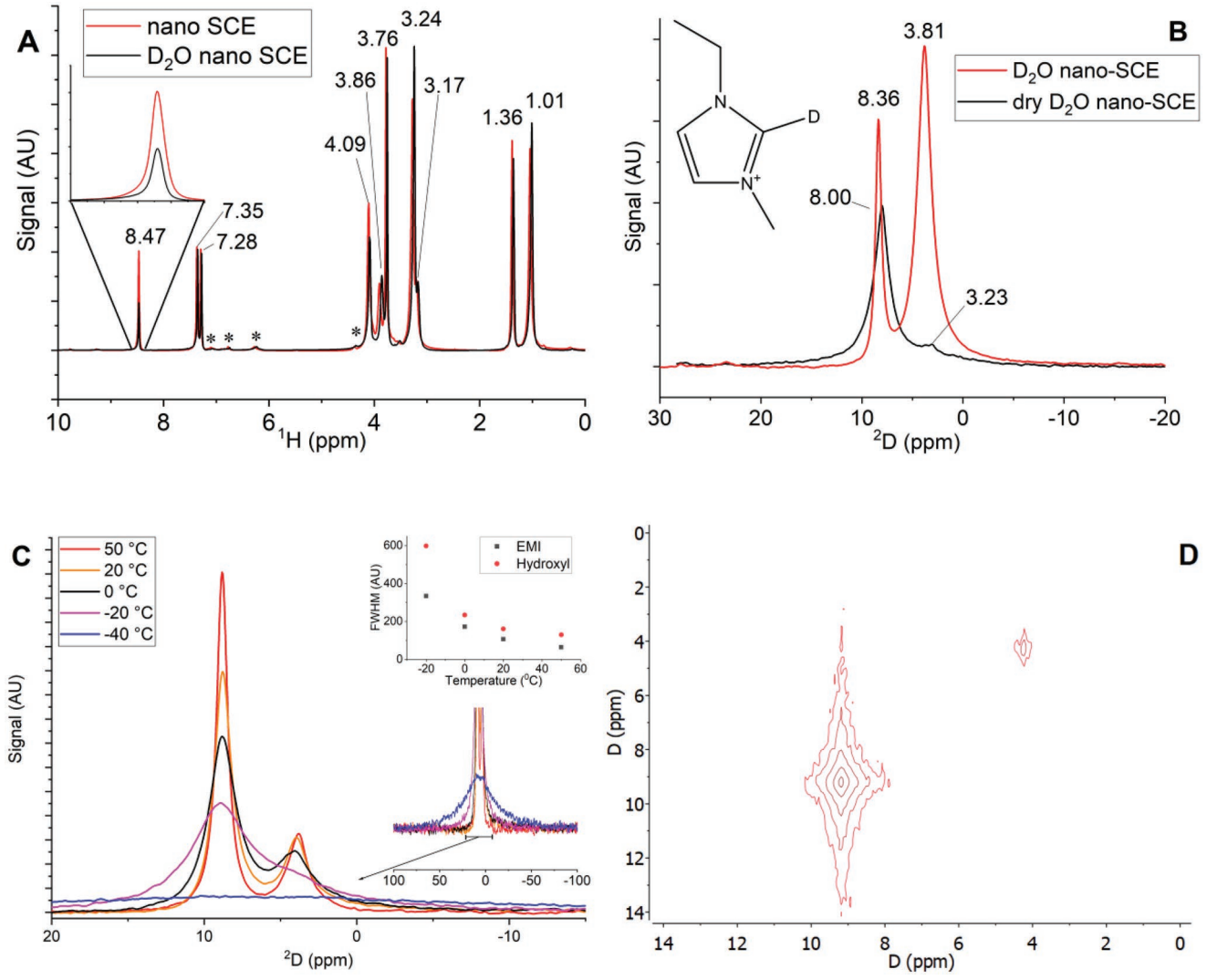

Figure 6. A) ^{1}H MAS-NMR spectra of nano-SCE prepared with H_2O (red) and D_2O (black) at room temperature and 1.5 kHz spinning frequency. Inset: the signal change in the D_2O derived nano-SCE indicates the proton in between the nitrogen groups in the EMI molecule has exchanged with deuterium. B) ^{2}D MAS-NMR spectra at 1.5 kHz at room temperature of nano-SCE (red) and dry-nano-SCE (black) produced with D_2O. C) Static ^{2}D spectra as function of temperature. Semi-dry nano-SCE is measured at temperatures 50 °C (red), 20 °C (orange), 0 °C (black), −20 °C (maroon), and −40 °C (blue). Line broadening as a result of a change in mobility is most dramatic from −20 to −40 °C. D) ^{2}D Exchange spectrum at 5 kHz at room temperature using Nuclear Overhauser Effect SpectroscopY (NOESY) of semi-dry nano-SCE using mixing times of 50 ms (blue).

more rapidly compared to the ionic liquid. The 3.81 ppm ^{2}D peak is associated with the hydroxyl groups of the ethanol-D6 and residual D_2O of the polymerization process and possibly silanol groups.[29] The peak is very broad compared to the ionic liquid peak, an indication that they are much less mobile compared to the ionic liquid. The EMI associated peak FWHM shows less broadening from 0 to −20 °C, at which temperatures the hydroxyl associated signal shows dramatic broadening (Figure 6C, inset right).

A quantification of the amount of hydroxyl groups in the material can be made using the deuterium signal. In dry nano-SCE, a majority of the deuterated water is removed which is observed by the reduced peak at 3.85 ppm in the ^{2}D MAS NMR spectrum (Figure 6B, black). The dry-nano-SCE shows a dramatic decrease of peaks at 1.15 and 3.35 ppm in the ^{1}H spectrum which corresponds to the loss of PGME. Also a slight peak shift of the EMI associated peaks at 7.31, 7.38, and 8.45 ppm is apparent (Figure S18, Supporting Information). The peak shift indicates de-shielding of the three protons of the imidazolium ring upon drying. The EMI group becomes more polar in the environment with lowered amounts of solvent. A concentration estimate can be made by comparing the peak intensities of the relative loss in intensity of the 8.36 ppm proton peak of the EMI to the increase in peak in the deuterium spectrum. Of the original EMI ^{1}H 8.47:7.35 ppm signal ratio, 47% of the signal is lost in the ^{1}H spectrum in the nano-SCE prepared with deuterated water. This signal amounts to 25% deuterium signal in the deuterium spectrum in the nano-SCE. For dry nano-SCE this amounts to ≈95% of the total peak area and increased broadening of the residual 5% of the signal indeed indicating immobilization of the water and other residuals with hydroxyl signatures upon extended drying. An indication of the solvation

of mobile molecules is that nano-SCE has a ratio of 0.66 EMI cations per hydroxyl bond and for dry-nano-SCE this becomes 38 EMI cations per hydroxyl bond.

Cycled nano-SCE shows broader peaks in the ^{1}H spectrum, indicating lower mobility (Figure S19, Supporting Information). The peak positions are maintained indicating the chemical composition of the ionic liquid is largely unaffected, although the peak around 3.42 ppm seems to indicate that some EMI has reacted to a dimer through the redox couple EMI-TFSI + Li → dim(EMI) + Li-TFSI. This is confirmed by a lower signal around 8.47 ppm, which cannot be caused by the proton–deuterium exchange as this sample was prepared using H_2O instead of D_2O.

Finally, ^{7}Li MAS NMR is utilized to ascertain the presence of different lithium ion environments that may explain the shift in signal shape. For the nano-SCE at temperatures above 4 °C, the ^{7}Li spectral peak at 1.5 kHz spinning rate shows an optimum spectral deconvolution with a single peak around −0.86 ppm (Figure S12, Supporting Information). This indicates the differences between the chemical environments are not distinguishable. Below 4 °C however two peaks can be distinguished and their intensity ratio does change. The broad environment becomes more abundant upon lowering the temperature. For example at −5 °C this becomes 0.46:0.54 broad:narrow and at −20 °C the ratio becomes 0.71:0.29. The broad environment has three times the FWHM compared to the narrow de-shielded environment due to motional narrowing.

In the dry-nano-SCE lithium ions are more isolated at room temperature, observable by a central chemical shift in the ^{7}Li MAS NMR spectrum from −0.86 to −1.04 ppm after extended drying (Figure S13, Supporting Information), indicating a more isolated ionic charge (Figure S13, Supporting Information, left). Two peaks can already be identified at room temperature of which the difference in chemical shift is only 0.039 ppm. The peak ratio is 0.58:0.42 more shielded:less shielded at room temperature. Trends in FWHM as function of temperature follow that of nano-SCE (Figures S13 and S17, Supporting Information). Both peaks are broadened compared to nano-SCE indicating lower mobility. The lower shielding, similar to the central protons in the EMI group indicate an overall more polar interaction with the TFSI group.

Similar to nano-SCE for dry nano-SCE there is a shift of ^{7}Li signal to a chemically shielded environment, indicating surface interactions become more abundant at low temperatures. However, for dry-nano-SCE only two environments can be deconvoluted and the signal already shifts to a more shielded state at higher temperatures compared to nano-SCE. At 20 °C almost all of the signal is in the chemically shielded region (Figure S17, Supporting Information) where in nano-SCE in this temperature range at least three lithium environments coexist (Figure S14, Supporting Information). This confirms that the volatile molecules extend the temperature range in which lithium remains in its mobile state.

3. Discussion and Conclusion

Nano-SCE shows promising characteristics by combining high conductivity with non-flammability and an elegant processing method. To date however, no nano-SCE has been prepared which outcompetes commercial available liquid electrolyte conductivities.[8] In this work the dry-nano-SCE shows a remarkable stable performance indicating that the SEI is stabilized at the gel/anode interface, an important characteristic for applicability. The dry-nano-SCE shows lower overpotentials compared to the semi-dry-nano-SCE. The cause of this originates from lower interfacial resistance while at the same time a good intrinsic conductivity is maintained. Limited SEI formation by the stabilizing structure of the silica backbone, combined with good contacting due to the flexible gel is thought to be the origin of the lowered interfacial resistance. For semi-dry nano-SCE a sharp increase in charge transfer resistance at elevated temperatures is shown to be in concert with lower bulk conductivities through temperature dependent EIS, indicating an increased rate of volatiles migration to the (reactive) lithium interface. The charge transfer resistance in dry nano-SCE is found to be stable after prolonged cycling, indicating formation of a stable SEI.

The mechanism of enhanced conduction is discussed in this work. We find that a lower solvation of lithium ions by the TFSI ions in samples containing volatiles is observed in line with Chen et al.[10] The amount of volatiles could be quantified by using the deuterium signal from deuterated water as reference with MAS NMR. Using NMR techniques we find however that an increased bulk mobility, rather than transfer of lithium ions from local sites by means of temporal dissociation from its counter ion is the dominant source of the increased lithium ion conduction. The latter process would involve a more dramatic change in activation energy which is not observed in this study (observable by for example varying the ILE/backbone ratio).[30] We show that desolvating groups enable lithium ion mobility at lower temperatures. Fast transfer processes probed using T_1 relaxation show a good fit with electrochemical impedance spectroscopy. With the combinatory approach of relaxometry and MAS NMR this work provides a complementary analysis of the structural and electrochemical features of this promising material.

4. Experimental Section

Synthesis of Nano-SCE: Nano-SCE was made in line with the synthesis method described by Chen et al.[10] except for the last drying steps, in which shorter and longer vacuum times were used. 0.33:1 mol:mol ratio Li-TFSI:EMI-TFSI (Solvionic, IL) was prepared in a glove box. Tetraethyl orthosilicate (>99%, Sigma Aldrich), 1-methoxy-2-propanol (99.5%, Sigma Aldrich), Deionized water or D_2O (99.9%, Sigma Aldrich), and IL were mixed in a ratio of 14:25:14:47 m/m%. After shaking the sample vigorously the liquid was poured over target material (porous cathode, current collector) or solidified in a glass vial. The mixture was solidified using >7 day room temperature (RT) polymerization at 44% rel. humidity. The gel was subsequently dried for 96 h at 800 mBarA pressure. The structure was further dried at 200 mBarA for 72 h. The dry nano-SCE sample without volatiles was obtained by drying the sample subsequently in 0.3 mBarA vacuum at 60 °C overnight. Semi-dry nano-SCE was obtained by sampling the container after 3.5 h during HVT. In the D_2O-nano-SCE samples instead of deionized water, deuterated water was added in the initial precursor solution.

Electrochemical Testing: EIS and galvanostatic tests were conducted using a vacuum clamp cell setup. A circular gel-sample holder was made by punching a ring with an inner diameter of 14 mm disc from a 0.80 mm thick sample cap. The gel sample was pressed in the ring shape, resulting in an 800 micron thick electrolyte disk. Lithium

discs of 15.4 mm diameter were used as electrodes. Electrochemical impedance spectroscopy was conducted using an Autolab PGSTAT302N potentiostat and a temperature programmable oven. Fitting of EIS data was performed using Zview. Cycling was performed using a MACCOR-4000 multichannel battery cell cycler in a climate controlled room.

NMR Spectroscopy: For NMR testing a Bruker Ascend 500 (B_0 = 11. 7 T) magnet equipped with a NEO console was used. The sample was filled in an air tight 4 mm rotor zirconia rotor with a vespel cap and inserted in a 4 mm triple resonance MAS NMR probe (Bruker). For ^{7}Li (194.37 MHz), $\pi/2$ pulse lengths of 3.48–4.50 µs (143.88 W) corresponding to an RF field strengths of 71.8–55.5 kHz were utilized. T_1's and $T_{1\rho}$'s measurements were performed under static conditions in the temperature range of –70 to 105 °C. Low temperature measurements were conducted by forcing the VT gas flow through liquid nitrogen as coolant and subsequent heating to the appropriate temperature. T_1 measurements were performed using the saturation recovery experiment, while $T_{1\rho}$ measurements were performed at spin lock fields of 12.5 and 30 kHz in the temperature range of –70 to 105 °C. The recycle delay was adjusted each time based on T_1 to ensure complete relaxation after every measurement. Relaxation measurement fitting was performed using the Dynamics Center module from Bruker. Temperature dependent relaxation rate fitting was conducted using the OriginPro 2019 software after deconvolution of the spectra. To evaluate the chemical composition of the various environments in which lithium ions are present in the nano-SCE, MAS NMR measurements were performed on ^{1}H (ω_0 = 500.130 MHz, $\pi/2_1$ = 3.15 µs, 170 W, ω_1 = 79.4 kHz), ^{2}D (ω_0 = 76.773 MHz, $\pi/2$ = 4.87 µs, 350 W, ω_1 = 51.4 kHz), and ^{7}Li (ω_0 = 194.370 MHz, $\pi/2$ = 3.48 µs, 143.88 W, ω_1 = 71.8 kHz). All MAS NMR measurements were performed at a 1.5 kHz spinning rate except NOESY performed at 5 kHz. Peak deconvolution was performed using the MestreNova software.

Scanning Electron Microscopy: SEM measurements were carried out using a JEOL6010 on additionally dried samples in which also liquid ionic liquid traces that were not bound in the nano-SCE were removed to prevent SEM contamination. Samples containing ionic liquid were soaked in a surplus of acetone and incubated several days to allow complete mixing and removal of any free ionic liquid not bound to the nano-SCE. The majority of the acetone was removed by careful pouring. The dilution, mixing and pouring off was repeated three times. The resulting material was subsequently dried overnight in a vacuum oven at 60 °C resulting in sand-like particles which were directly measured.

Supporting Information

Supporting Information is available from the Wiley Online Library or from the author.

Acknowledgements

This project has received funding from the European Union's Horizon 2020 research and innovation programme under grant agreement No. 875557. Neither the European Commission nor any person acting on behalf of the Commission is responsible for how the following information is used. The views expressed in this publication are the sole responsibility of the authors and do not necessarily reflect the views of the European Commission.

Conflict of Interest

The authors declare no conflict of interest.

Data Availability Statement

The data that support the findings of this study are available from the corresponding author upon reasonable request.

Keywords

diffusivity, ionic conductivity, ionogel, nanoporous silica, nuclear magnetic resonance spectroscopy

Received: July 26, 2022
Revised: October 1, 2022
Published online:

[1] J. Le Bideau, J.-B. Ducros, P. Soudan, D. Guyomard, *Adv. Funct. Mater.* **2011**, *21*, 4073.
[2] X. Chen, P. M. Vereecken, *Adv. Mater. Interfaces* **2019**, *6*, 1800899.
[3] S. Li, N. Li, C. Sun, *Inorg. Chem. Front.* **2021**, *8*, 361.
[4] Q. Yi, W. Zhang, T. Wang, J. Han, C. Sun, *Energy Environ. Mater.* **2022**. https://doi.org/10.1002/eem2.12289
[5] T. Wang, X. Zhang, N. Yuan, C. Sun, *Chem. Eng. J.* **2023**, *451*, 138819.
[6] G. Qiu, C. Sun, *New J. Chem.* **2020**, *44*, 1817.
[7] C. Sun, J. Liu, Y. Gong, D. P. Wilkinson, J. Zhang, *Nano Energy* **2017**, *33*, 363.
[8] A. Sagara, X. Chen, K. B. Gandrud, M. Murata, M. Mees, Y. Kaneko, H. Arase, P. M. Vereecken, *J. Electrochem. Soc.* **2020**, *167*, 070549.
[9] A. Sagara, H. Yabe, X. Chen, P. M. Vereecken, A. Uedono, *Microporous Mesoporous Mater.* **2020**, *295*, 109964.
[10] X. Chen, B. Put, A. Sagara, K. Gandrud, M. Murata, J. A. Steele, H. Yabe, T. Hantschel, M. Roeffaers, M. Tomiyama, H. Arase, Y. Kaneko, M. Shimada, M. Mees, P. M. Vereecken, *Sci. Adv.* **2020**, *6*, eaav3400.
[11] A. Guyomard-Lack, P.-E. Delannoy, N. Dupré, C. V. Cerclier, B. Humbert, J. Le Bideau, *Phys. Chem. Chem. Phys.* **2014**, *16*, 23639.
[12] N. K. Jayakody, C. C. Fraenza, S. G. Greenbaum, D. Ashby, B. S. Dunn, *J. Phys. Chem. B* **2020**, *124*, 6843.
[13] M. Uitz, V. Epp, P. Bottke, M. Wilkening, *J. Electroceram.* **2017**, *38*, 142.
[14] A. F. McDowell, N. L. Adolphi, C. A. Sholl, *J. Phys. Condens. Matter.* **2001**, *13*, 9799.
[15] N. Bloembergen, E. M. Purcell, R. V. Pound, *Phys. Rev.* **1948**, *73*, 679.
[16] R. A. Assink, B. D. Kay, *J. Non-Cryst. Solids* **1988**, *99*, 359.
[17] A. Issa, A. Luyt, *Polymers* **2019**, *11*, 537.
[18] J. Cihlář, *Colloids Surf., A* **1993**, *70*, 239.
[19] A. M. Buckley, M. Greenblatt, *J. Chem. Educ.* **1994**, *71*, 599.
[20] J. Moškon, J. Žuntar, S. D. Talian, R. Dominko, M. Gaberšček, *J. Electrochem. Soc.* **2020**, *167*, 140539.
[21] A. M. Stephan, *Eur. Polym. J.* **2006**, *42*, 21.
[22] A. Rachocki, E. Andrzejewska, A. Dembna, J. Tritt-Goc, *Eur. Polym. J.* **2015**, *71*, 210.
[23] A. Guyomard-Lack, B. Said, N. Dupré, A. Galarneau, J. Le Bideau, *New J. Chem.* **2016**, *40*, 4269.
[24] M. Chintapalli, K. Timachova, K. R. Olson, S. J. Mecham, D. Devaux, J. M. DeSimone, N. P. Balsara, *Macromolecules* **2016**, *49*, 3508.
[25] C. D'Agostino, M. D. Mantle, C. L. Mullan, C. Hardacre, L. F. Gladden, *ChemPhysChem* **2018**, *19*, 1081.
[26] K. Fujii, Y. Soejima, Y. Kyoshoin, S. Fukuda, R. Kanzaki, Y. Umebayashi, T. Yamaguchi, S. Ishiguro, T. Takamuku, *J. Phys. Chem. B* **2008**, *112*, 4329.
[27] H. Saruwatari, T. Kuboki, T. Kishi, S. Mikoshiba, N. Takami, *J. Power Sources* **2010**, *195*, 1495.
[28] C. A. Ober, R. B. Gupta, *Ind. Eng. Chem. Res.* **2012**, *51*, 2524.
[29] I. S. Protsak, Y. M. Morozov, W. Dong, Z. Le, D. Zhang, I. M. Henderson, *Nanoscale Res. Lett.* **2019**, *14*, 160.
[30] C.-H. Tsao, H.-M. Su, H.-T. Huang, P.-L. Kuo, H. Teng, *J. Membr. Sci.* **2019**, *572*, 382.
[31] A. Delgado, M. F. García-Sánchez, J.-C. M'Peko, A. R. Ruiz-Salvador, G. Rodríguez-Gattorno, Y. Echevarría, F. Fernández-Gutierrez, *J. Chem. Educ.* **2003**, *80*, 1062.